

# Electric-field controlled spin reversal in a quantum dot with ferromagnetic contacts

J.R. HAUPTMANN<sup>1\*</sup>, J. PAASKE<sup>1</sup> AND P.E. LINDELOF<sup>1</sup>

<sup>1</sup>The Niels Bohr Institute & The Nano-Science Center, University of Copenhagen, DK-2100 Copenhagen, Denmark

\*e-mail: rahlf@fys.ku.dk.

(Dated: July 3, 2021)

arXiv:0711.0320v1 [cond-mat.mes-hall] 2 Nov 2007

Manipulation of the spin-states of a quantum dot by purely electrical means is a highly desirable property of fundamental importance for the development of spintronic devices such as spin-filters, spin-transistors and single-spin memory as well as for solid-state qubits<sup>1,2,3,4,5,6</sup>. An electrically gated quantum dot in the Coulomb blockade regime can be tuned to hold a single unpaired spin-1/2, which is routinely spin-polarized by an applied magnetic field<sup>7</sup>. Using ferromagnetic electrodes, however, the properties of the quantum dot become directly spin-dependent and it has been demonstrated that the ferromagnetic electrodes induce a local exchange-field which polarizes the localized spin in the absence of any external fields<sup>8,9</sup>. Here we report on the experimental realization of this tunneling-induced spin-splitting in a carbon nanotube quantum dot coupled to ferromagnetic nickel-electrodes. We study the intermediate coupling regime in which single-electron states remain well defined, but with sufficiently good tunnel-contacts to give rise to a sizable exchange-field. Since charge transport in this regime is dominated by the Kondo-effect, we can utilize this sharp many-body resonance to read off the local spin-polarization from the measured bias-spectroscopy. We show that the exchange-field can be compensated by an external magnetic field, thus restoring a zero-bias Kondo-resonance<sup>9</sup>, and we demonstrate that the exchange-field itself, and hence the local spin-polarization, can be tuned and reversed merely by tuning the gate-voltage<sup>10,11</sup>. This demonstrates a very direct electrical control over the spin-state of a quantum dot which, in contrast to an applied magnetic field, allows for rapid spin-reversal with a very localized addressing.

Since the discovery of carbon nanotubes they have been intensively studied for their unique electrical properties. Their high Fermi-velocity and small spin-orbit coupling make them particularly well-suited for spintronics applications utilizing the transformation of spin-information into electrical signals. Spin-valve effects in nano-junctions with a carbon nanotube (CNT) spanning two ferromagnetic electrodes have already been observed<sup>12,13,14</sup>, and a strong gate-dependence of the tunnel magneto-resistance has been demonstrated for carbon nanotube quantum dots in both the Coulomb blockade, and the Fabry-Perot regime<sup>12</sup>.

In the intermediate coupling regime, odd numbered quantum dots exhibit the Kondo effect seen as a pronounced zero-bias conductance peak at temperatures below a character-

istic Kondo temperature,  $T_K^{15,16,17}$ . This effect relies on the conduction electrons being able to flip the spin of the dot during successive cotunneling-events and is therefore expected to be sensitive to spin-polarization of the electrodes. As pointed out by Martinek et al.<sup>9</sup>, quantum charge-fluctuations of the dot will renormalize the single-particle energy-levels in a spin-dependent manner and thereby break the spin-degeneracy on the dot, causing the zero-bias Kondo peak to split in two. This tunneling-induced exchange-field splitting has since been seen by Pasupathy *et al.*<sup>8</sup> in an electromigrated Ni-gap holding a  $C_{60}$ -molecule.

A singly occupied level residing just below the Fermi-energy of the leads is strongly shifted by virtual tunneling *out of* the dot, whereas a level deep below the Fermi-energy (by almost the charging-energy) is shifted by tunneling of electrons *into* the dot. For spin-polarized electrodes having a difference in the density of spin-up, and spin-down states, this implies a spin-splitting of the dot level where sign and size depends on the applied gate-voltage, i.e. the position of the level below the Fermi-energy. At the particle-hole symmetric point right between the empty and doubly occupied states the spin-degeneracy is expected to be intact<sup>18</sup>. In a material like Ni, however, one expects the band structure to be energy dependent and to have a Stoner splitting, this will break the particle-hole symmetry and therefore shift the spin-degeneracy point away from the middle of the diamond<sup>10,11</sup>. Basically all the theoretical predictions for this pronounced gate-dependence of the local spin-states are experimentally verified by the transport-measurements presented below.

The CNTs were grown by chemical vapor deposition on a  $\text{SiO}_2$  wafer with a highly doped Si back-gate. The ferromagnetic leads were made of pure Ni in strips of thickness  $\sim 60$  nm, widths  $\sim 300$ -1000 nm and separated by 200-400 nm. All measurements were made in a  $^3\text{He}/^4\text{He}$  dilution refrigerator, with a base-temperature of 30 mK, corresponding to a minimum electron temperature of 80 mK, and using a standard AC-setup with asymmetric bias. A magnetic field was applied in the direction of the Ni-leads in the plane of the electrodes as shown in figure 1a. We observe a clear even-odd effect with a zero-bias anomaly in every second Coulomb diamond indicating a spin-1/2 Kondo effect with a typical Kondo temperature,  $T_K \sim 1$  K. Many of the observed Kondo anomalies showed a gate-dependent splitting and here we discuss two different devices for which this dependence is particularly clear, in the supplement two other examples are shown.

Magnetic force microscopy images of devices similar to the ones measured indicate that the CNT quantum dot is most likely coupled to one single domain in both source, and drain

electrode. Applying a strong magnetic field serves partly to align the two contact-domains and partly to provide a Zeeman-splitting of the local spin. Figure 2 shows the conductance vs. bias-voltage and external field, measured for a gate-voltage tuned to the middle of an odd occupied Coulomb blockade valley in the Kondo regime. Device 1 (figure 2**a,b**) shows a simple linear behavior in which the single-domain magnetization and hence the exchange field,  $\mathbf{B}_{ex}$ , is aligned with the external field,  $\mathbf{B}$ . The exchange field can therefore be completely compensated and the zero-bias Kondo peak is seen to be restored at  $B \sim \pm 1.12$  T, giving an indirect measure of the exchange-field at this gate-voltage. In device 2 (figure 2**c,d**), on the other hand, the Kondo peak is never fully restored and the splitting merely reaches a minimum at  $B \sim \pm 0.6$  T. This indicates that the exchange-field lies at an angle to the external field, and fitting the B-dependence of the peak-splitting by  $e\Delta V = g\mu_B|\mathbf{B} + \mathbf{B}_{ex}|$ , we find this angle to be  $\angle(\mathbf{B}, \mathbf{B}_{ex}) \sim 25^\circ$  (cf. supplementary material).

Figure 2 was recorded by sweeping the field from large negative to large positive values, a sudden decrease(increase) of the splitting is clearly visible at small negative(positive) fields. A similar switching was observed in Ref. 8 and can be ascribed to a sudden switching from parallel (P) to anti-parallel (AP) configuration of the contact-domains driven by domain interactions (cf. supplementary material). In the AP-configuration the tunnel-induced exchange-field is nearly canceled, unless the couplings to source, and drain-electrodes are very different. In terms of the conduction-electron spin-polarization,  $P = (\nu_{F\uparrow} - \nu_{F\downarrow})/\nu_F$ , and the tunnel-broadening,  $\Gamma_{s(d)} = \pi\nu_F|t_{s(d)}|^2$ , where  $\nu_F = \nu_{F\uparrow} + \nu_{F\downarrow}$  denotes the density of states (DOS) in the leads and  $t_{s(d)}$  is the tunneling amplitude to source(drain), one expects<sup>8,19</sup> that  $g\mu_B B_{ex}^{(AP/P)} = \Delta\varepsilon_{ex}^{(AP/P)} = aP(\Gamma_s \mp \Gamma_d)$ . Comparing now the exchange-fields in P, and AP-configuration we deduce that  $\Gamma_s/\Gamma_d \sim 3$ , this corresponds to a zero-bias Kondo peak height of  $(2e^2/h)4\Gamma_s\Gamma_d/(\Gamma_s + \Gamma_d)^2 = 1.5 e^2/h$  roughly consistent to the value of  $1.4 e^2/h$ , measured on device 1 in the middle of the Coulomb blockade diamond for a fully compensating magnetic field near  $B = \pm 1.12$  T.

In a Coulomb blockade diamond with an odd number of electrons, the left, and right charge-degeneracy points correspond to respectively emptying the dot or filling it by one extra electron. With a finite spin-polarization in the leads, tunneling of majority-spins, spin-up say, will be favored by the higher-density of states and a dot-state of spin-up will therefore be shifted further down in energy than a spin-down state, as long as one is closer to the left hand side (l.h.s.) of the diamond. Due to the Pauli-principle, the majority-spins can

only tunnel into the dot if the residing electron is in a spin-down state. It is therefore the spin down state which is lowered the most near the right hand side (r.h.s.) of the diamond. This simple mechanism of level-renormalization, illustrated in figure **3a-c**, is encoded in the exchange-field, given to good accuracy by

$$\Delta\varepsilon_{ex}(\varepsilon_d) = e\Delta_{st} + (P\Gamma/\pi) \ln(|\varepsilon_d|/|U + \varepsilon_d|) \quad (1)$$

to leading order in the tunneling-amplitude<sup>11</sup> and assuming a constant density of states.  $U$  is the charging-energy and  $\varepsilon_d$  is the dot-level-position which is proportional to the gate-voltage. Notice the strong negative and positive logarithmic corrections for  $\varepsilon_d$  close to 0 or  $-U$ , respectively (corresponding to left, and right borders of the diamond). In the middle of the diamond,  $\varepsilon_d = -U/2$ , the exchange-field is zero except for a constant term,  $\Delta_{st}$ , which reflects a Stoner-splitting between the spin-up and spin-down bands<sup>10,11</sup>. Notice that possible stray-fields from the magnetic contacts would also contribute with a gate-independent spin-splitting (cf. supplementary material).

Depending on the magnitude of  $\Delta_{st}$ , Equation (1) predicts a change of the ground state spin direction as the localized level is moved from  $\varepsilon_d = 0$  to  $\varepsilon_d = -U/2$ . Such a spin reversal can be observed in figure **3d-g** and occurs where the Kondo ridges cross and the spin states are degenerate<sup>20</sup>. The movement of the conductance peak (red dot) as function of magnetic field, seen in figure **3d-g**, confirms that the ground-state spin can indeed be reversed by changing the gate-voltage. Furthermore, the direction of the motion shows that it is predominantly spin-up (i.e. the spin along the external magnetic field) electrons which tunnel on and off the dot, giving a ground-state with spin-up at the l.h.s of the diamond and spin-down at the r.h.s. This confirms earlier observations in conventional superconducting tunnel-junctions<sup>21,22</sup> indicating that the tunneling electrons in Ni have majority-spin, i.e. positive polarization. Most likely, the more mobile  $s$ -electrons taking part in the tunneling are spin-polarized by their hybridization with the localized  $d$ -electrons<sup>23,24</sup>.

In order to substantiate the detailed gate-voltage dependence of the exchange-field, we have extracted the peak-positions from plots like those in figures **3d-g** and fitted them by  $(\Delta\varepsilon_{ex}(\varepsilon_d) - g\mu_B B)/e$  with  $\Delta\varepsilon_{ex}$  given by equation (1). The result is shown in figure **4a** where the inset shows  $\Delta_{st} - g\mu_B B/e$  as a function of  $B$ . The slope of the line corresponds to  $g = 2$  as expected for a carbon nanotube. The white ridge in Figure **4b** traces the magnetic field dependence of the gate-voltage at which the spin states are degenerate, showing a gratifying

resemblance to the theory-plots presented in Refs. 10,11. Inverting equation (1) and using the fitting-parameters deduced from figure 4a, we arrive at the parameter free fit seen as the black line in figure 4b.

- 
- <sup>1</sup> Wolf, S. A. *et al.* Spintronics: a spin-based electronics vision for the future. *Science* **294**, 1488-1495 (2001).
  - <sup>2</sup> Awschalom, D. D. & Flatté, M. E. Challenges for semiconductor spintronics. *Nature* **3**, 153 (2007).
  - <sup>3</sup> Ohno, H., *et al.* Electric-field control of ferromagnetism. *Nature* **408**, 944 (2000).
  - <sup>4</sup> Recher, P., Sukhorukov, E. V. & Loss, D. Quantum Dot as Spin Filter and Spin Memory. *Phys. Rev. Lett.* **85**, 1962 (2000).
  - <sup>5</sup> Folk, J. A., Potok, R. M., Marcus, C. M. & Umansky, V. A Gate-Controlled Bidirectional Spin Filter Using Quantum Coherence. *Science* **299**, 679 (2003).
  - <sup>6</sup> Elzerman, J. M., Hanson, R., Willems van Beveren, L. H., Witkamp, B., Vandersypen, L. M. K. & Kouwenhoven, L. P. Single-shot read-out of an individual electron spin in a quantum dot. *Nature* **430**, 431 (2004).
  - <sup>7</sup> Lindelof, P. E., Borggreen, J., Jensen, A., Nygård, J. & Poulsen, P. R. Electron Spin in Single Wall Carbon Nanotubes. *Physica Scripta* **T102**, 22 (2002).
  - <sup>8</sup> Patsupathy, A. N. *et al.* The Kondo effect in the presence of ferromagnetism. *Science* **306**, 86 (2004).
  - <sup>9</sup> Martinek, J. *et al.* Kondo effect in Quantum Dots coupled to Ferromagnetic Leads. *Phys. Rev. Lett.* **91**, 127203 (2003).
  - <sup>10</sup> Martinek, J. *et al.* Gate controlled splitting in quantum dots with ferromagnetic leads in the Kondo regime. *Phys. Rev. B* **72**, 121302 (2005).
  - <sup>11</sup> Sindel, M. *et al.* Kondo quantum dot coupled to ferromagnetic leads: a study by numerical renormalization group technique. *Phys. Rev. B* **76**, 45321 (2007).
  - <sup>12</sup> Sahoo, S. *et al.* Electric field control of spin transport. *Nature Physics* **1**, 99 (2005).
  - <sup>13</sup> Jensen, A., Hauptmann, J. R., Nygård, J. & Lindelof, P. E. Magnetoresistance in ferromagnetically contacted single-wall carbon nanotubes. *Phys. Rev. B* **72**, 35419 (2005).
  - <sup>14</sup> Hueso, L. E. *et al.* Transformation of spin information into large electrical signals using carbon

- nanotubes. *Nature* **445**, 410 (2007).
- <sup>15</sup> Glazman, L. & Raikh, M. Resonant Kondo transparency of a barrier with quasilocal impurity states. *JETP Letters* **47**, 452-455 (1988).
- <sup>16</sup> Goldhaber-Gordon, D. *et al.* Kondo effect in a single-electron transistor. *Nature* **391**, 156 (1998).
- <sup>17</sup> Nygård, J., Cobden, D. H. & Lindelof, P. E. Kondo physics in carbon nanotubes. *Nature* **408**, 342 (2000).
- <sup>18</sup> Choi, M. S., Sanchez, D. & Lopez, R. Kondo effect in quantum dot coupled to ferromagnetic leads: a numerical renormalization group analysis. *Phys. Rev. Lett.* **92**, 56601 (2004).
- <sup>19</sup> Utsumi, Y., Martinek, J., Schön, G., Imamura, H. & Maekawa, S. Nonequilibrium Kondo effect in a quantum dot coupled to ferromagnetic leads. *Phys. Rev. B* **71**, 245116 (2005).
- <sup>20</sup> Note that these plots have been recorded prior to a switch in device 1, whereas all other measurements taken on device 1 were recorded after. We present these plots since they bring out most clearly the movement of the degeneracy point. The corresponding plots recorded after the gate-switch are shown in the supplementary material and are qualitatively similar
- <sup>21</sup> Tedrow, P. M. & Meservey, R. Spin-Dependent Tunneling into Ferromagnetic Nickel. *Phys. Rev. Lett.* **26**, 192 (1971).
- <sup>22</sup> Kim, T. H. & Moodera, J. S. Large spin polarization in epitaxial and polycrystalline Ni films. *Phys. Rev. B* **69**, 20403(R) (2004).
- <sup>23</sup> Mazin, I. I. How to Define and Calculate the Degree of Spin Polarization in Ferromagnets. *Phys. Rev. Lett.* **83**, 1427 (1999).
- <sup>24</sup> Tsymbal, E. Y. & Pettifor, D. G. Modelling of spin-polarized electron tunnelling from 3d ferromagnets. *J. Phys.: Condens. Matter* **9**, L411 (1997).

## Acknowledgements

We thank R. Gunnarsson, L. Borda, K. Flensberg, P. Hedegård, and C. M. Marcus for discussions. For financial support we thank Danish Agency for Science Technology and Innovation (FTP 274-05-0178) and EU projects SECOQC and CARDEQ.

## Competing financial interests

The authors declare that they have no competing financial interests.

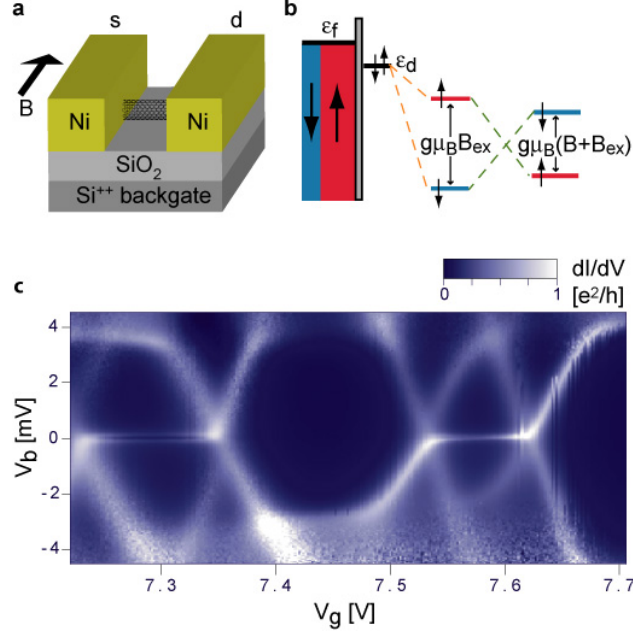


FIG. 1: Carbon nanotube quantum dot with magnetic contacts. **a**, Schematic view of the device comprised of a segment of carbon-nanotube on a Si/SiO<sub>2</sub> substrate, contacted by two Ni-leads in a standard field-effect configuration. A magnetic field is applied along the leads in the plane of the substrate. **b**, The local spin-states are split partly by the tunneling-induced exchange-field,  $B_{ex}$  (in orange) that depends on gate voltage and partly by the external magnetic field  $B$  (in green) resulting from the applied field  $B$ . **c**, Plot of the differential conductance  $dI/dV$  as a function of gate  $V_g$ , and bias-voltage  $V_b$  measured on device 2. A series of 4 Coulomb diamonds can be observed with a pronounced zero-bias spin-1/2 Kondo peak in the two diamonds corresponding to odd-numbered occupation.

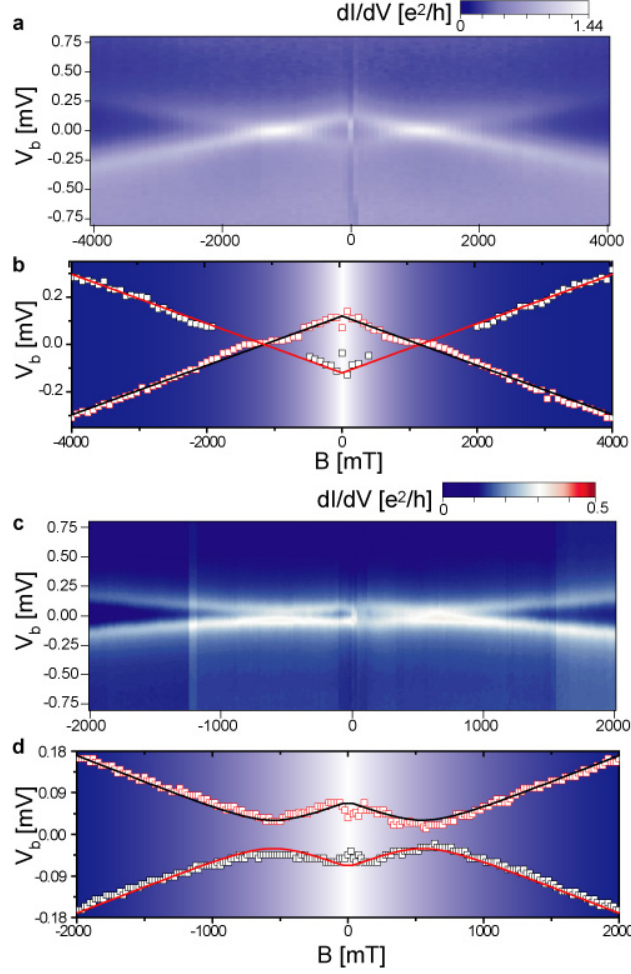


FIG. 2: Kondo peak splitting as a function of applied magnetic field at fixed gate-voltage. **a**,  $dI/dV$  vs. bias-voltage and magnetic field measured on device 1, sweeping from -4 T to 4 T. The plot is recorded in the middle of an odd numbered spin-1/2 Kondo diamond. The observed splitting of the Kondo peak is due to the the exchange field  $B_{ex}$  and external field  $B$ . At  $B \sim \pm 1.12$  T the external field is compensating the exchange-field and restoring the zero-bias Kondo peak. A sudden change in  $dI/dV$  is observed at  $B \sim -80$  mT due to a switching of one of the two contact-domains. At  $B \sim 80$  mT the other domain has flipped and we are back in a parallel configuration. **b**, Plot of the peak positions from **a**, offset with  $V_b = 5 \mu\text{V}$  to symmetrize the plot. The black, and red lines are fits to the peak positions and have a slope of  $\pm 1.04 \times 10^{-4} \text{ V/T}$  corresponding to  $g \sim 1.8$ . **c**, Plot as in **a**, measured on device 2, sweeping from -2 T to 2 T. In this device the exchange-field is never completely compensated, indicating a misalignment of the domain magnetization direction and the applied magnetic field,  $\mathbf{B}$ . A domain-switch causes a sudden jump in the splitting at  $B \lesssim |40|$  mT. **d**, Peak positions from **c**, offset by  $V_b = 12 \mu\text{V}$ . The black, and red lines are fits to the plots where the domain magnetization direction is at an angle of  $25^\circ$  to the external field (see text).

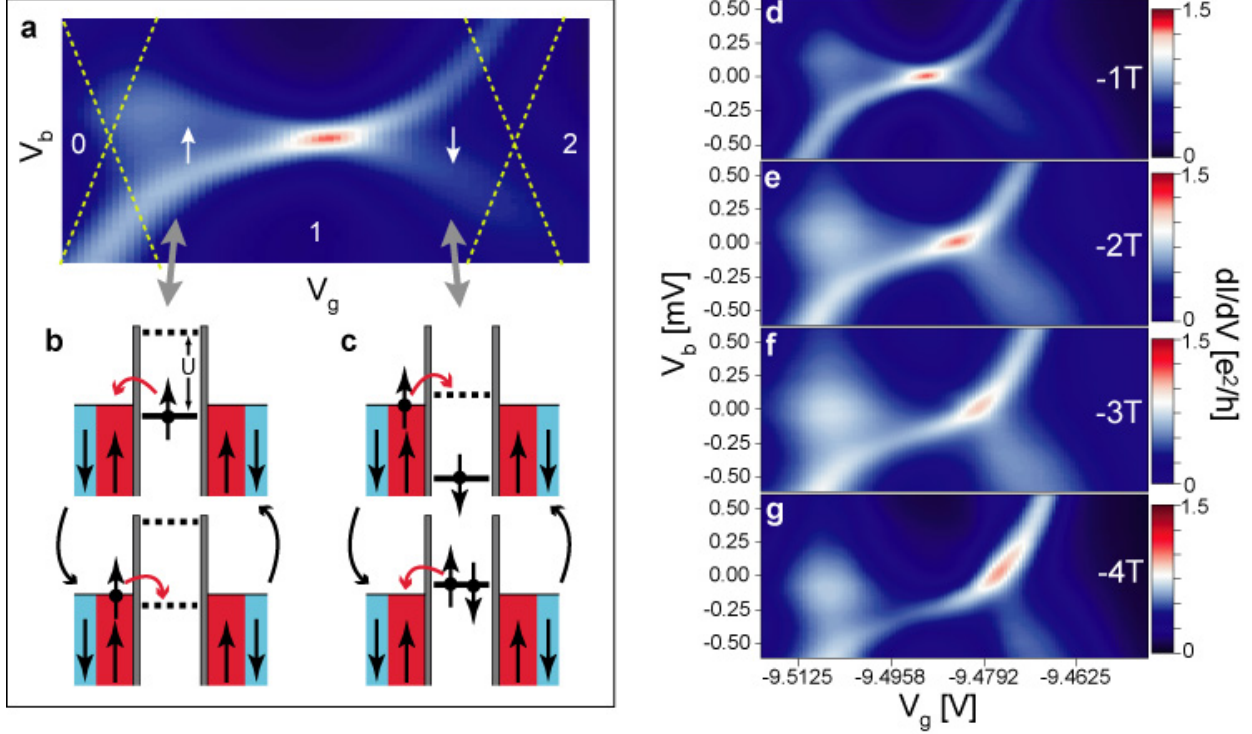


FIG. 3: Gate dependence of the spin-states probed by the Kondo effect. **a**, Plot from **d**, with yellow dotted lines added to indicate the diamond edges. Numbers indicate the number of electrons in one orbital state. Arrows indicates the local spin ground-state which changes with the exchange-field as the gate-voltage is varied. These spin ground-states on the dot are consistent with the observation in **d-g**, that the conductance peak (red spot) moves to the right as the field is increased. **b**, **c**, Illustration of the virtual tunneling-processes leading to a spin-up(down) ground-state in the left(right) side of the dot, the full drawn lines are filled states and the dotted lines are empty states. Upper and lower diagrams correspond to ground, and excited states. Red spin-up represents the majority s-electron-band in the leads, hybridizing the most with the dot-electrons. **d-g**, Plots of  $dI/dV$  as a function of gate, and bias-voltage, measured on device 1 in different external magnetic fields. The Kondo peak is clearly seen to have a gate-dependent splitting. Full compensation in the middle of the diamond is obtained close to  $B = -1\text{T}$  as seen in **d**.

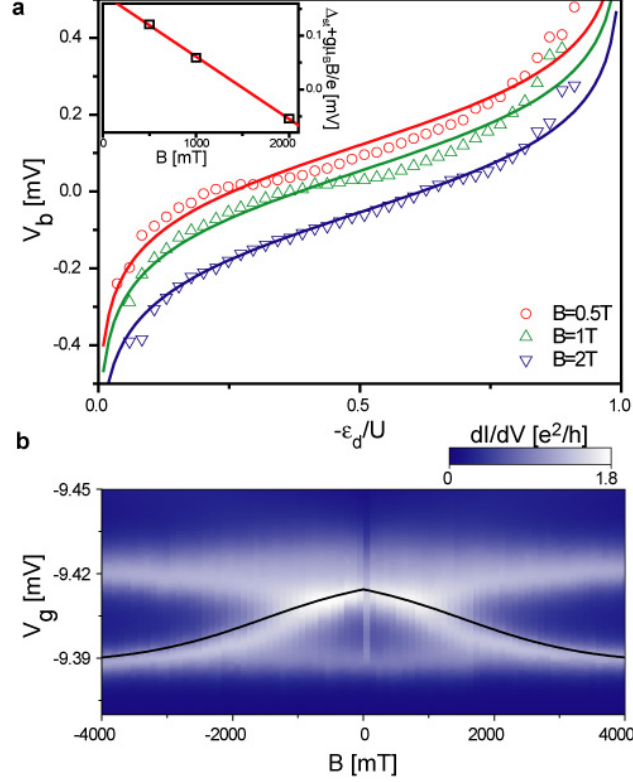


FIG. 4: Gate dependence of the exchange-field for different applied magnetic fields. **a**, Scatter-plot of the dominant Kondo peak position, in bias-voltage, as a function of level-position  $\varepsilon_d(\propto V_g)$  gate-voltage for device 1. Peak-positions are read off from plots similar to those in figure 3d-g (cf. supplementary material). The different colors correspond to different magnetic fields. The gate-axis has been displaced and normalized with the charging energy such that the dot is emptied at  $\varepsilon_d = 0$  and becomes doubly occupied at  $\varepsilon_d = -U$ . Full lines are fits to the data, using  $(\Delta\varepsilon_{ex} - g\mu_B B)/e$  defined by Eq.(1) and with  $g = 2$ . All three curves are fitted by  $P\Gamma = 0.113 * \pi$ . The inset shows a fit to the gate-independent term  $\Delta_{st} - g\mu_B B/e$  with  $\Delta_{st} = 0.18$  mV. **b**,  $dI/dV$  as a function of gate-voltage and magnetic field measured at zero bias voltage. The two nearly horizontal lines are Coulomb peaks and the white line moving from the lower to the upper peak as  $B$  is lowered, is a Kondo peak, thus mapping out where the spin states are degenerate. The black line is described by the function  $\varepsilon_d = U/(e^{(e\Delta_{st} - g\mu_B B)\pi/P\Gamma} + 1) - c$  where  $c$  is a constant determined by the first Coulomb peak and  $U$  is the charging energy.  $c$  and  $U$  are read off from the plot while the other constants are determined from the fits in **a**. Notice that, like in figure 2, a domain switch is seen at  $|B| \lesssim 80$  mT.

# Supplementary material for "Electric-field controlled spin reversal in a quantum dot with ferromagnetic contacts"

## I. DOMAIN SWITCHING AND STRAY-FIELDS

Magnetic force microscopy images of devices similar to the ones measured, reveal a typical domain-size of  $V_{dom} = 100 \times 500 \times 50 \text{ nm}^3$ , which suggests that the carbon nanotube quantum dot is most likely coupled to one single domain in both source, and drain electrodes. Using the saturation magnetization for Ni,  $M_s = 0.61\text{T}/\mu_0$ , the magnetic moment of a single contact-domain can be estimated by  $V_{dom}M_s$ . With 200 nm between the electrodes, this gives a crude estimate of the dipole-dipole interaction energy of the two contact-domains with an energy-gain of roughly 200 eV between the parallel (P) and anti-parallel (AP) configurations. Starting in the P-configuration for a large applied magnetic field, this in turn implies a transition to AP-configuration once the external field becomes smaller than some 30 mT. The switching from P to AP observed in article-figures **2a,c** occurs at fields smaller than 80 mT for device 1 and close to 40 mT for device 2. Article-figures **2a,c** were recorded with a resolution in  $B$  of 80 mT and 10 mT, respectively. This simple estimate of course neglects all intra-lead domain-interactions, which cannot a priori be assumed to be less important.

From this we can also estimate the stray-field at the middle between the two electrodes. In the AP-configuration it is close to zero and in the P-configuration it must be roughly  $B_{stray} \sim 100 \text{ mT}$ , i.e. a factor of 10 and 5, respectively, smaller than the tunneling-induced exchange-fields which we read off from article-figures **2a,c**. We note that this rather crude estimate is comparable in magnitude to the estimates made in Refs. 1,2,3. Notice also that stray-fields cannot account for the gate dependence observed in article-figures **3d-g**.

The fact that the exchange-field cannot be completely compensated by the external field in device 2 is interpreted as a misalignment of  $\mathbf{B}_{ex}$  and  $\mathbf{B}$ . Since bulk Ni has only weak magnetic anisotropy, this is most likely due to the reduced geometry and surface roughness of the leads. The fit shown in article-figure **2d** takes a fixed direction of the magnetization which is found to be  $\angle(\mathbf{B}, \mathbf{B}_{ex}) \sim 25^\circ$ . We have also tried to make another fit with a finite anisotropy barrier, using a simple Stoner-Wohlfarth model where the magnetic energy of the

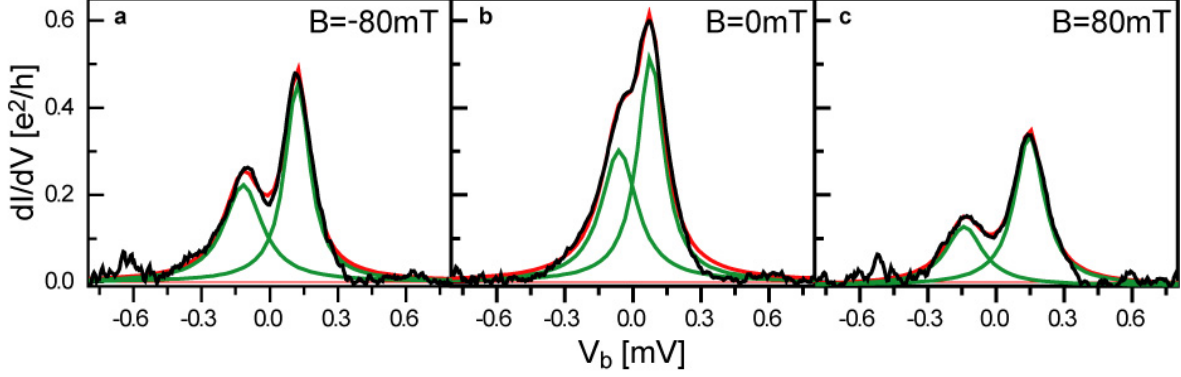


FIG. 5: Plots of  $dI/dV$  as a function of bias voltage for  $B = -80$  mT,  $B = 0$  mT and  $B = 80$  mT the plots are line-cuts through the plot shown in article-figure 1a, measured on device 1. The black curves are the measurements with a baseline subtracted. The green lines are Lorentzian fits to the peaks and the red lines are the resulting double-peak fits. The center-to-center distance of the Lorentzians in each of the three plots gives the splitting of the spin-up and spin-down states on the dot. The splittings are 0.239, 0.139 and 0.287 mV for **a**, **b** and **c**, respectively, corresponding to domain configurations which are **a** parallel, **b** anti-parallel and **c** parallel.

system is given by

$$E = K \sin^2(\theta - \phi) - BM \cos(\phi), \quad (2)$$

in terms of applied field  $B$  and magnetization  $M$  at a relative angle  $\phi$ , together with an angle  $\theta$  between an easy-axis and the applied field.  $K$  parameterizes the anisotropy barrier, thus allowing the magnetization to align with  $\mathbf{B}$  for large enough values of  $BM/K$ . Minimizing this energy as a function of angle for a given applied field gives a hysteretic magnetization curve from which we can then infer the sum of applied, and exchange-field to determine the spin-splitting as a function of  $B$ . Nevertheless, this fit performed no better than the far simpler fit to a fixed angle.

## II. ADDITIONAL PLOTS FOR DEVICES 1 AND 2

### A. Device 1

The ratio of the couplings to respectively source and drain electrodes can be estimated from the formula

$$\frac{\Gamma_s}{\Gamma_d} = \frac{\Delta V_P - 2g\mu_B B/e + \Delta V_{AP}}{\Delta V_P - 2g\mu_B B/e - \Delta V_{AP}}, \quad (3)$$

where  $V_P(V_{AP})$  denotes the splittings in the parallel (antiparallel) configuration which are read off from figure 5. This gives the estimate  $\Gamma_s/\Gamma_d \sim 3$ , cited in the main paper.

The plots in figure 6 shows the differential conduction as a function of gate and bias voltage measured at different magnetic fields. The measurements are made on device 1 after a switch, i.e. a sudden, permanent change in the device behavior. Notice that the crossing of the Kondo ridges moves from left to right as the magnetic field is increased. It is these measurements that the scatter and fits in article-figure 4a are made from. Note that the plot measured at  $B = -1$  T has also been fitted but is not shown in article-figure 4a since it is placed right on top of  $B = 1$  T. The plot made at  $B = 0$  T is not included in the fitting since the domain configuration is expected to be different. The point corresponding to  $B = 1$  T in the inset of article-figure 4a is really the average of the fitted constants, 0.065 mV and 0.053 mV, obtained at  $B = -1$  T and  $B = 1$  T, respectively.

### B. Device 2

The plot shown in figure 7 shows the differential conductance as a function of gate, and bias voltage measured at different magnetic fields. The slopes of the Kondo ridges in **a**, **b** and in **e** are clearly opposite, although the measurements at intermediate magnetic fields (**c**, **d**) show no crossing of the Kondo ridges. We ascribe this to a misalignment of the domain magnetization direction (and therefore the exchange field) and the external magnetic field.

## III. PLOTS FOR DEVICES 3 AND 4

Figure 8 shows the differential conduction as a function of gate, and bias voltage. Two Kondo ridges near zero bias can be observed and henceforth we shall refer to the corresponding odd-numbered Coulomb-blockade diamonds as devices 3 and 4, respectively. These mea-

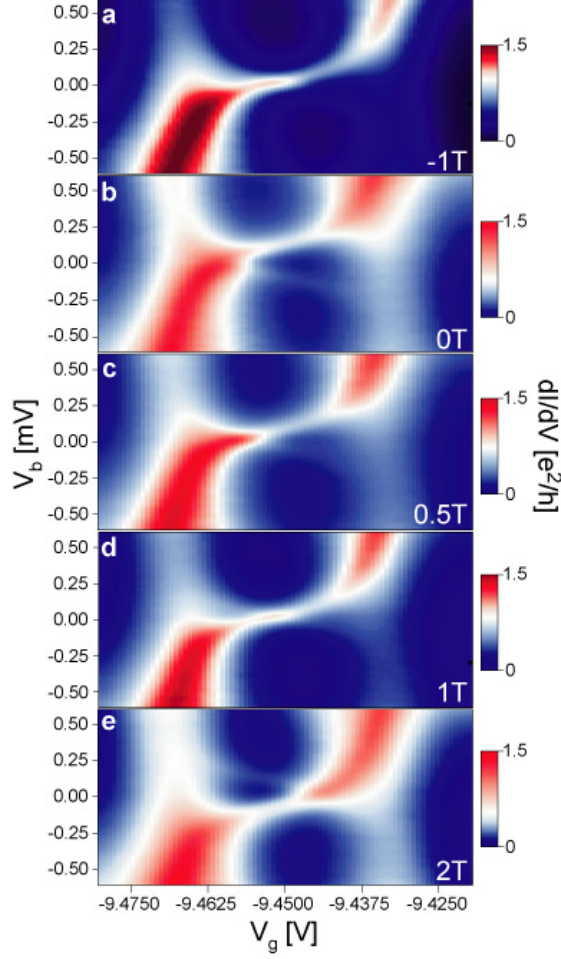


FIG. 6: Gate-dependence of the spin-states probed by the split Kondo-peak measured on device 1 post switch. **a-e** show the differential conductance as a function of gate, and bias-voltage measured at different magnetic fields. Notice that the crossings of the Kondo ridges move to the right as the magnetic field is increased. It is from these plots the scatters and the fits in article-figure 4 **a** is made.

measurements are made on the same sample as device 1 but off-set in gate voltage by roughly 20 V.

Figure 9 shows  $dI/dV$  as a function of bias voltage and magnetic field. The measurements are made close to the middle of the Coulomb-blockade diamond in device 3. A linear splitting of the Kondo peak with magnetic field can be observed, as would be expected since this device should be contacted by the same domains as device 1 and the domain configuration and magnetization direction in the leads should be independent of the gate voltage.

Figure 10c shows a zoom-in on the Kondo ridges, measured at  $B = -1$  T. A gate de-

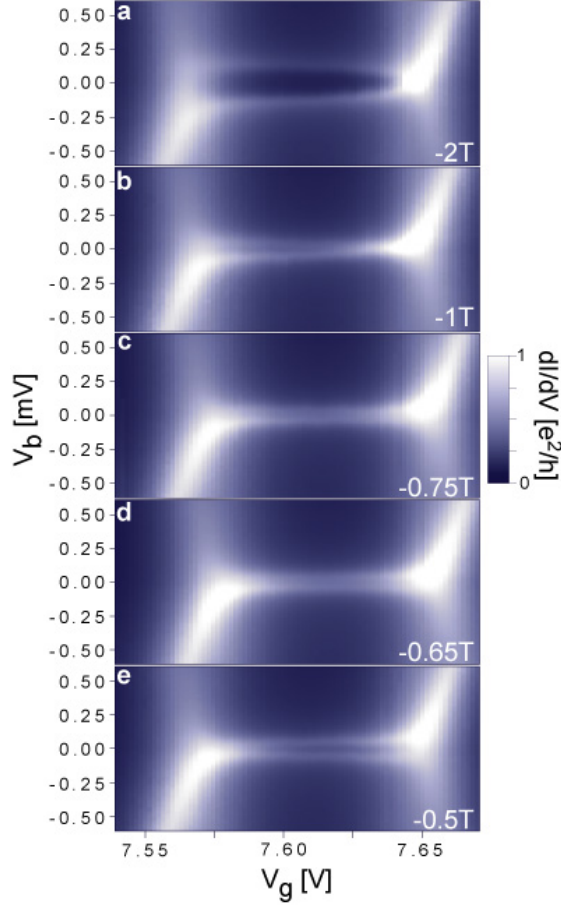


FIG. 7: Gate dependence of the spin-states probed by the Kondo effect measured on device 2. **a-e** show the differential conductance as a function of gate and bias voltage measured at different magnetic fields. Notice that the Kondo ridges do not cross in any of the plots. This is interpreted as a misalignment of the domains and the external field.

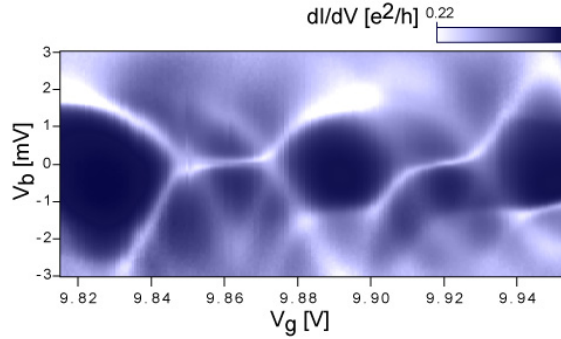


FIG. 8: Five Coulomb diamonds with a Kondo resonance in every second. The plot show the differential conductance as a function of gate and bias voltage.

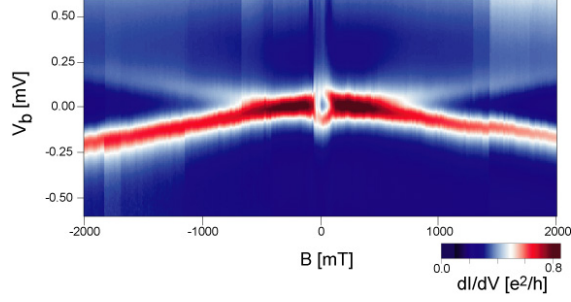


FIG. 9: Kondo peak splitting as a function of magnetic field at fixed gate voltage measured on device 3. The plots shows the differential conductance as a function of bias and magnetic field, swept from 2 T to -2 T.

pendent splitting of the Kondo resonance is clearly observed in both device. The different slopes indicate a change in  $\Gamma = \Gamma_s + \Gamma_d$  from one Kondo resonance too the next, most likely due to a difference in couplings to the two orbitals in the CNT.

The splittings of the Kondo peaks have been read off and plotted in figure 10**a,b**. The lines are fits to the scatter-plots and the different colors correspond to different external magnetic fields. The fitted values used for  $P\Gamma/\pi$  are 0.045 and 0.117 meV for the groups of fits in **a** and **b**, respectively. The insets in both figures show  $\Delta_{st} + g\mu_B B$  as function of  $B$ . The two linear fits yield a slope of  $9.9 \times 10^{-5}$  (**a**) and  $1.0 \times 10^{-4}$  (**b**), corresponding to a  $g$ -factor of 1.7 and 1.8, respectively.

Figure 11 shows  $dI/dV$  as function of gate voltage and magnetic field. Panels **a** and **b** correspond to devices 3 and 4, respectively. The black line is plotted using the procedure described in the caption of article-figure 4**b**, now with parameters obtained from figure 10.

---

<sup>1</sup> Patsupathy, A. N. *et al.* The Kondo effect in the presence of ferromagnetism. *Science* **306**, 86 (2004).

<sup>2</sup> Sahoo, S. *et al.* Electric field control of spin transport. *Nature Physics* **1**, 99 (2005).

<sup>3</sup> Meier, L., Salis, G., Ellenberger, C., Ensslin, K., Gini, E. Stray-field-induced modification of coherent spin dynamics. *Appl. Phys. Lett.* **88**, 172501 (2006).

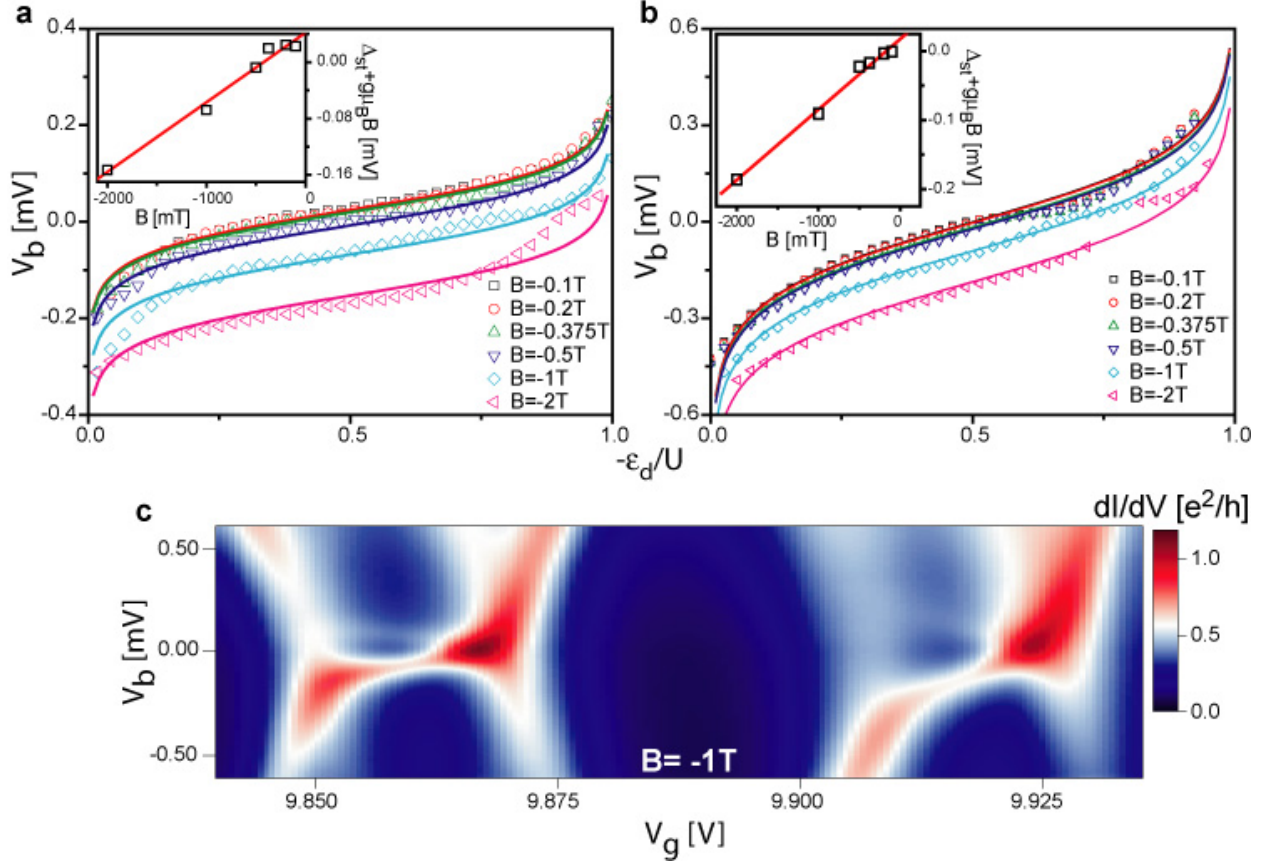


FIG. 10: Gate dependence of the exchange field for different applied magnetic fields measured on **a** device 3 and **b** device 4. **c** Show the differential conduction as a function of bias and gate voltage the measurement are made with an external field of -1 T. Four Coulomb peaks and two Kondo resonances are observed the 1st resonance corresponds to device 3 and the 2nd to device 4. **a**, **b** shows the scatter plot of the peak position read off from measurement like the one shown in **c**, where the gate voltage have been normalized with the charging energy. The different colors and shapes corresponds to different external magnetic fields. The lines are fits to the scatters. The insert shows the fitting constant  $\Delta_{st} + g\mu_B B$  for the different magnetic fields and a linear fit to these points.

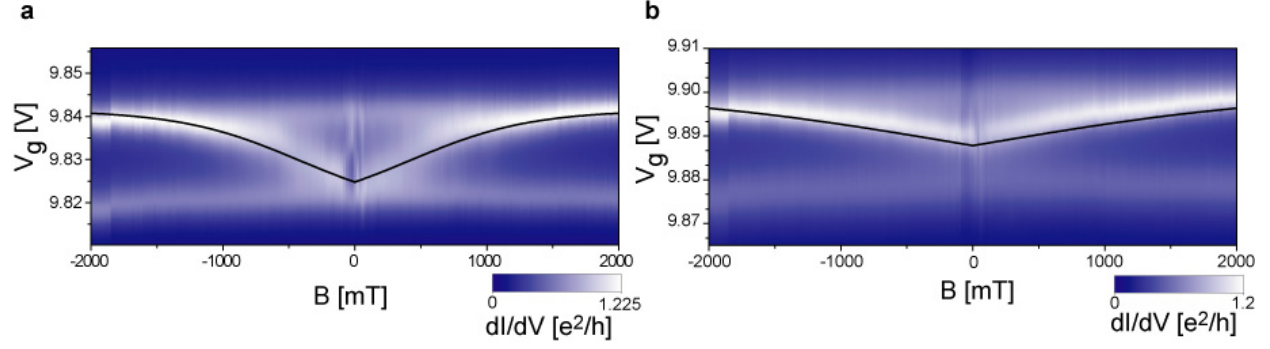


FIG. 11: Gate dependence of the exchange field at zero bias. The plots shows the differential conduction as a function of gate voltage and external magnetic field for device 3 **a** and device 4 **b**. The two horizontal lines in each plot are due to Coulomb peaks. The white line crossing from one peak to the other **a** or halfway between them **b** are mapping out the Kondo peak movement (the point where the spin states are degenerate) as a function of magnetic field. The black line are parameter free fit where the constant have been found from the fits in figure 10. Similar to the parameter free fit shown in article-figure 4**b**.